Available online at www.sciencedirect.com
ScienceDirect
International Journal of Heat and Mass Transfer 50 (2007) 2002–2018
International Journal of HEAT and MASS TRANSFER
www.elsevier.com/locate/ijhmt

Heat transfer augmentation in a two-sided lid-driven differentially heated square cavity utilizing nanofluids

Raj Kamal Tiwari [1], Manab Kumar Das *

Department of Mechanical Engineering, Indian Institute of Technology Guwahati, North Guwahati, Guwahati 781 039, Assam, India

Received 4 April 2006; received in revised form 21 September 2006
Available online 8 December 2006

Abstract

The behaviour of nanofluids is investigated numerically inside a two-sided lid-driven differentially heated square cavity to gain insight into convective recirculation and flow processes induced by a nanofluid. A model is developed to analyze the behaviour of nanofluids taking into account the solid volume fraction χ. The transport equations are solved numerically with finite volume approach using SIMPLE algorithm. Comparisons with previously published work on the basis of special cases are performed and found to be in excellent agreement. The left and the right moving walls are maintained at different constant temperatures while the upper and the bottom walls are thermally insulated. Three case were considered depending on the direction of the moving walls. Governing parameters were $0.01 < Ri < 100$ but due to space constraints only the results for $0.1 < Ri < 10$ are presented. It is found that both the Richardson number and the direction of the moving walls affect the fluid flow and heat transfer in the cavity. Copper–Water nanofluid is used with $Pr = 6.2$ and solid volume fraction χ is varied as 0.0%, 8%, 16% and 20%. Detailed results are presented for flow pattern and heat transfer curves.

Keywords: Nanofluid; Mixed convection; Collocated grid; Heat transfer augmentation

1. Introduction

Low thermal conductivity of conventional heat transfer fluids such as water, oil, and ethylene glycol mixture is a primary limitation in enhancing the performance and the compactness of many engineering electronic devices. To overcome this drawback, there is a strong motivation to develop advanced heat transfer fluids with substantially higher conductivities to enhance thermal characteristics. As such an innovative way in improving thermal conductivities of a fluid is to suspend metallic nanoparticles within it. The resulting mixture referred to as a nanofluid possesses a substantially larger thermal conductivity compared to that of the traditional fluids [1]. The presence of the nanoparticles in the fluids increases appreciably the effective thermal conductivity of the fluid and consequently enhances the heat transfer characteristics.

The natural convection problem in a differentially heated square cavity is numerically simulated by Khanafer et al. [2] considering the dispersion effect. In their methodology, the dispersion constant "C" is to be determined by experimental data observation. Amiri and Vafai [3] discussed this model and used it for porous media. Khaled and Vafai [4] investigated the effect of controlled dispersion in a channel. The maximum Nusselt number for analyzed distributions of the dispersive elements are found to be 21% higher than that with uniformly distributed dispersive elements for a uniform flow. The volume fraction distribution that maximizes the heat transfer is governed by the flow and thermal conditions as well as the properties of dispersive elements. Using different correlations analytically, Chein and Huang [5] have analyzed microchannel heat sink for Nusselt number and pressure drop based on Reynolds number and pumping power. Koo and Kleinstreuer [6]

* Corresponding author. Tel.: +91 361 2582655; fax: +91 361 2690762.
E-mail addresses: mr_rajkt@yahoo.com (R.K. Tiwari), manab@iitg.ernet.in (M.K. Das).
[1] Present address: Engineering and Research Center, Tata Motors Limited, Lucknow 226 019, India.

0017-9310/$ - see front matter © 2006 Elsevier Ltd. All rights reserved.
doi:10.1016/j.ijheatmasstransfer.2006.09.034

Nomenclature

i	x-direction grid point
j	y-direction grid point
k_f	thermal conductivity of the fluid, W/m K
k_s	thermal conductivity of the solid, W/m K
Nu	local Nusselt number
$\overline{Nu}$	average Nusselt number
n	time level
Pr	Prandtl number, $\frac{\nu_f}{\alpha_f}$
Re	Reynolds number for the fluid
t^*	dimensional time, s
t	non-dimensional time
u^*, v^*	dimensional velocity components along (x^*, y^*) axes, m/s
u, v	dimensionless velocity components along (x, y) axes
V_p	velocity of the moving lid, m/s
x^*, y^*	dimensional Cartesian co-ordinates, m
x, y	dimensionless Cartesian co-ordinates

Greek symbols

α	thermal diffusivity, m^2/s
β_f	fluid thermal expansion coefficient
β_s	solid expansion coefficient
ε	convergence criterion
κ	excess thermal-conductivity enhancement coefficient
ν	kinematic viscosity, m^2/s
χ	solid volume fraction

Subscripts

c	cold wall
eff	effective
f	fluid
h	hot wall
nf	nanofluid
0	reference value
s	solid

Superscript

*	dimensional term

have used Brownian motion based-thermal conductivity and viscosity to numerically simulate the microheat sink. Additionally they considered the viscous dissipation term. They suggested that a high-Prandtl number base fluid and a high aspect ratio channel should be used for better heat transfer performance. Roy et al. [7] has considered the case of radial flow cooling system for numerical simulation. For physical properties calculation they obtained a correlations by curve fitting on the experimental data and found that nanofluids increased the wall shear stress in a considerable way. Maiga et al. [8] have numerically simulated nanofluid behaviour in a uniformly heated tube for laminar as well as turbulent flow using approximated correlations for experimental data. They found that for turbulent flow regime, the heat transfer enhancement due to nanoparticles becomes more important with the increase of the Reynolds number. In another study, Maiga et al. [9] numerically simulated nanofluids in forced convection flows and solved the problems of uniformly heated tube and a system of parallel, coaxial and heated disks. They found that both the through flow Reynolds number and the gap between disks have insignificant effect on the heat transfer enhancement of nanofluids.

Fluid flow and heat transfer in a rectangular or a square cavity driven by buoyancy and shear have been studied extensively in the literature [10,11]. Mixed convection problem with lid-driven flows in enclosures are encountered in a variety of engineering applications including cooling of electronic devices, furnaces, lubrication technologies, chemical processing equipment, drying technologies, etc. Combination of buoyancy forces due to temperature gradient and forced convection due to shear results in a mixed convection heat transfer, which is a complex phenomenon due to the interaction of these forces.

To investigate the heat transfer enhancement by very fine particles suspended in a fluid, two main approaches have been adopted in the literature. The first one is the two-phase model that takes into account the fluid and solid phase role in the heat transfer process. The second one is the single-phase model where both the fluid phase and the solid particles are in thermal equilibrium state and flow with the same local velocity. Several issues are involved while studying the heat transfer enhancement utilizing nanofluids. These issues are like gravity, Brownian motion, layering at the interface between solid and liquid, clustering of the nanoparticles, ballistic phono transport through the particles and the friction between the fluid and the solid particles. The phenomena of sedimentation, dispersion and Brownian diffusion may coexist in the main flow of a nanofluid. In the absence of any suitable theoretical studies and experimental data in the literature to investigate these issues, the existing macroscopic two-phase model is not applicable for analyzing nanofluids [2,12]. If the main interest is focused on the heat transfer process, the modified single-phase, accounting for some of the above factors, is more convenient than the two-phase model. Also, the superior characteristics of the nanofluid allow it to behave more like a fluid rather than the conventional solid–fluid

mixtures. Modeling the effective thermal conductivity poses a challenge while studying the heat transfer enhancement using nanofluids. Maxwell's model [13] predicted that the effective thermal conductivity of suspensions containing spherical particles increases with an increase in the volume fraction of the solid particles. Hamilton and Crosser [14] developed an expression for the effective thermal conductivity of two-component mixtures taking into consideration the liquid and solid particle thermal conductivities, particle volume fraction and an empirical scaling factor to account for the different shapes of the particles.

Although prospects of nanofluids is very promising, there is still a dearth of enough research. To the best knowledge of the authors, the problem of heat transfer enhancement in a two-sided lid-driven differentially heated square cavity filled with nanofluids has not been analyzed. This problem may be encountered in a number of electronic cooling and MEMS applications. The present study is focussed on the analysis of several pertinent parameters on the heat transfer characteristics of nanofluids within the enclosure. In the present study, a time marching incompressible flow solver has been applied for simulating the flow features of nanofluids for a range of solid volume fraction (χ) values and Richardson number (Ri).

2. Mathematical formulation

Consider a two-sided lid-driven square cavity filled with a nanofluid. The vertical lids have different constant temperatures. The horizontal walls are assumed to be insulated, non-conducting, and impermeable to mass transfer. Three different cases were considered as shown in Fig. 1. In case I, the left wall (cold) is moving up while right wall (hot) is moving down. In case II, the left wall is moving down while the right wall is moving upwards, and in case III both the walls are moving upwards. In all the three cases, the moving walls have the same speed and gravitational force direction is parallel to the moving walls. The nanofluid in the enclosure is Newtonian, incompressible, and laminar. The nanoparticles are assumed to have a uniform shape and size. Moreover, it is assumed that both the fluid phase and nanoparticles are in thermal equilibrium state and they flow at the same velocity. The thermophysical properties of the nanofluid are assumed to be constant except for the density variation in the buoyancy force, which is based on the Boussinesq approximation.

We have considered the continuity, momentum and energy equations for a Newtonian, Fourier constant property fluid governing an unsteady, two-dimensional flow. It is further assumed that radiation heat transfer among sides is negligible with respect to other modes of heat transfer. Under the assumption of constant thermal properties, the Navier–Stokes equation for an unsteady, incompressible, two-dimensional flow are

Continuity equation:

$$\frac{\partial u^*}{\partial x^*}+\frac{\partial v^*}{\partial y^*}=0 \tag{1}$$

x-momentum equation:

$$\frac{\partial u^*}{\partial t^*}+\frac{\partial (u^{*2})}{\partial x^*}+\frac{\partial (u^*v^*)}{\partial y^*}=-\frac{1}{\rho_{\mathrm{nf},0}}\frac{\partial p^*}{\partial x^*}+\frac{\mu_{\mathrm{eff}}}{\rho_{\mathrm{nf},0}}\left(\frac{\partial^2 u^*}{\partial x^{*2}}+\frac{\partial^2 u^*}{\partial y^{*2}}\right) \tag{2}$$

y-momentum equation:

$$\frac{\partial v^*}{\partial t^*}+\frac{\partial (u^*v^*)}{\partial x^*}+\frac{\partial (v^{*2})}{\partial y^*}=-\frac{1}{\rho_{\mathrm{nf},0}}\frac{\partial p^*}{\partial y^*}+\frac{\mu_{\mathrm{eff}}}{\rho_{\mathrm{nf},0}}\left(\frac{\partial^2 v^*}{\partial x^{*2}}+\frac{\partial^2 v^*}{\partial y^{*2}}\right)+\frac{1}{\rho_{\mathrm{nf},0}}[\chi\rho_{\mathrm{s},0}\beta_{\mathrm{s}}+(1-\chi)\rho_{\mathrm{f},0}\beta_{\mathrm{f}}]g(T-T_{\mathrm{c}}) \tag{3}$$

Energy equation:

$$\frac{\partial T^*}{\partial t^*}+\frac{\partial (u^*T^*)}{\partial x^*}+\frac{\partial (v^*T^*)}{\partial y^*}=\alpha_{\mathrm{nf}}\left(\frac{\partial^2 T^*}{\partial x^{*2}}+\frac{\partial^2 T^*}{\partial y^{*2}}\right) \tag{4}$$

where

$$\alpha_{\mathrm{nf}}=k_{\mathrm{eff}}/(\rho C_p)_{\mathrm{nf},0}$$

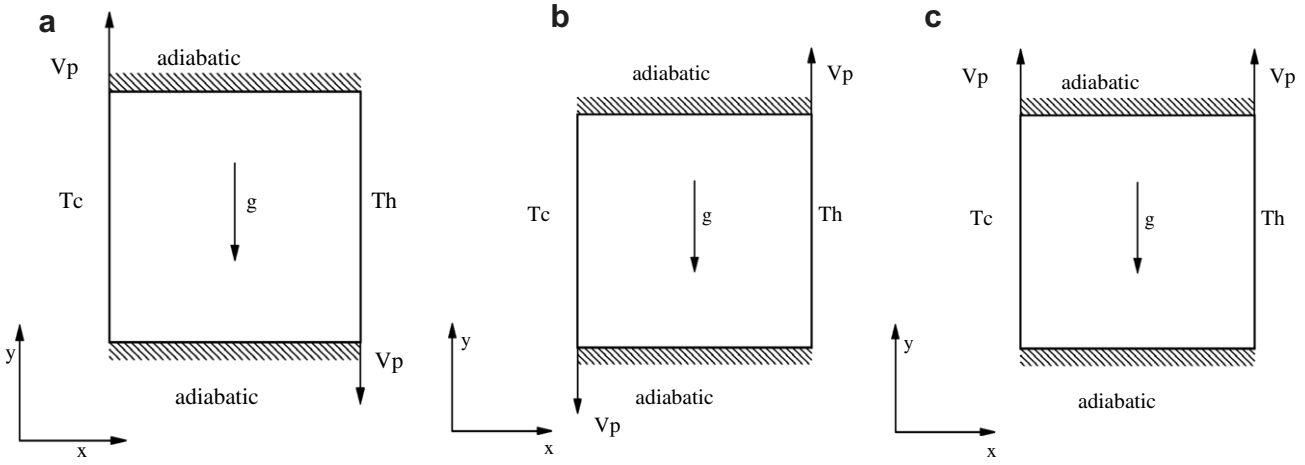

Fig. 1. Physical model for three cases and the co-ordinate system: (a) Case I; (b) Case II; (c) Case III.

The viscosity of the nanofluid can be estimated with the existing relations for the two-phase mixture. The equation given by Brinkman [15] has been used as the relation for effective viscosity in this problem, as given by

$$\mu_{\text{eff}} = \frac{\mu_{\text{f}}}{(1-\chi)^{2.5}} \tag{5}$$

Xuan and Li [16] have experimentally measured the apparent viscosity of the transformer oil–water nanofluid and of the water–copper nanofluid in the temperature range of 20–50 °C. The experimental results reveal relatively good agreement with Brinkman's theory.

The effective density of the nanofluid at reference temperature is

$$\rho_{\text{nf},0} = (1-\chi)\rho_{\text{f},0} + \chi\rho_{\text{s},0} \tag{6}$$

and the heat capacitance of nanofluid is

$$(\rho C_p)_{\text{nf}} = (1-\chi)(\rho C_p)_{\text{f}} + \chi(\rho C_p)_{\text{s}} \tag{7}$$

as given by Xuan and Li [17]. The effective thermal conductivity of fluid can be determined by Maxwell–Garnett's (MG model) self-consistent approximation model. For the two-component entity of spherical-particle suspension, the MG model gives

$$\frac{k_{\text{eff}}}{k_{\text{f}}} = \frac{(k_{\text{s}}+2k_{\text{f}}) - 2\chi(k_{\text{f}}-k_{\text{s}})}{(k_{\text{s}}+2k_{\text{f}}) + \chi(k_{\text{f}}-k_{\text{s}})} \tag{8}$$

In the absence of any convenient formula, the calculation of effective thermal conductivity can be obtained from the above equation. For further analysis, it is convenient to introduce the excess thermal-conductivity enhancement coefficient κ, defined as

$$\kappa = \frac{k_{\text{eff}} - k_{\text{f}}}{k_{\text{HC}} - k_{\text{f}}} \tag{9}$$

In the above definition, κ is simply the ratio of measured thermal conductivity increase divided by the increase predicted by the Hamilton–Crosser (HC) theory. Consequently, $\kappa = 1$ indicates agreement with the macroscopic theory, and $\kappa > 1$ measures the magnitude of thermal-conductivity enhancement. The above equations can be converted to non-dimensional form, using the following dimensionless parameters:

$$x = \frac{x^*}{H}, \quad y = \frac{y^*}{H}, \quad u = \frac{u^*}{V_{\text{p}}}, \quad v = \frac{v^*}{V_{\text{p}}},$$
$$p = \frac{p^*}{(\rho V_{\text{p}}^2)}, \quad T = \frac{T^* - T_{\text{c}}^*}{\Delta T^*},$$
$$Gr = \frac{g\beta H^3 \Delta T^*}{v_{\text{f}}^2}, \quad Re = \frac{V_{\text{p}} H}{v_{\text{f}}}, \quad Pr = \frac{v_{\text{f}}}{\alpha_{\text{f}}}$$

The governing equations can now be written in dimensionless form as follows:

Continuity equation:

$$\frac{\partial u}{\partial x} + \frac{\partial v}{\partial y} = 0 \tag{10}$$

x-momentum equation:

$$\frac{\partial u}{\partial t} + \frac{\partial (u^2)}{\partial x} + \frac{\partial (uv)}{\partial y} = -\frac{\rho_{\text{f},0}}{\rho_{\text{nf},0}}\frac{\partial p}{\partial x} + \frac{1}{v_{\text{f}} \cdot Re}\frac{\mu_{\text{eff}}}{\rho_{\text{nf},0}}\left(\frac{\partial^2 u}{\partial x^2} + \frac{\partial^2 u}{\partial y^2}\right) \tag{11}$$

y-momentum equation:

$$\frac{\partial v}{\partial t} + \frac{\partial (uv)}{\partial x} + \frac{\partial v^2}{\partial y} = -\frac{\rho_{\text{f},0}}{\rho_{\text{nf},0}}\frac{\partial p}{\partial y} + \frac{1}{v_{\text{f}} \cdot Re}\frac{\mu_{\text{eff}}}{\rho_{\text{nf},0}}\left(\frac{\partial^2 v}{\partial x^2} + \frac{\partial^2 v}{\partial y^2}\right) + \frac{\chi\rho_{\text{s}}\beta_{\text{s}} + (1-\chi)\rho_{\text{f}}\beta_{\text{f}}}{\beta_{\text{f}}\rho_{\text{nf},0}} RiT \tag{12}$$

Energy equation:

$$\frac{\partial T}{\partial t} + \frac{\partial (uT)}{\partial x} + \frac{\partial (vT)}{\partial y} = \frac{\alpha_{\text{nf}}}{\alpha_{\text{f}}}\frac{1}{Pr \cdot Re}\left[\frac{\partial^2 T}{\partial x^2} + \frac{\partial^2 T}{\partial y^2}\right] \tag{13}$$

Boundary conditions are isothermal on the vertical moving lids and adiabatic on the horizontal walls. On the horizontal walls, u and v velocities are zero and the lids have a constant velocity. The relevant boundary conditions are given as follows:

$$\begin{aligned}
&u = 0,\ v = 1 \quad \text{or} \quad (v = -1) \quad \text{for } x = 0 \text{ and } 0 \leqslant y \leqslant 1\\
&u = 0,\ v = 1 \quad \text{or} \quad (v = -1) \quad \text{and} \quad T = 1.0\\
&\quad \text{for } x = 1 \text{ and } 0 \leqslant y \leqslant 1\\
&u = v = 0 \quad \text{and} \quad \frac{\partial T}{\partial y} = 0 \quad \text{for } y = 0 \text{ and } 0 \leqslant x \leqslant 1\\
&u = v = 0 \quad \text{and} \quad \frac{\partial T}{\partial y} = 0 \quad \text{for } y = 1 \text{ and } 0 \leqslant x \leqslant 1
\end{aligned} \tag{14}$$

The Nusselt number of the nanofluids is expected to depend on a number of factors such as thermal conductivity and heat capacitance of both the pure fluid and the ultrafine particles, the volume fraction of the suspended particles, the flow structure and the viscosity of the nanofluid. The local variation of the Nusselt number of the nanofluid can be expressed as

$$Nu = \frac{Q}{Q_{\text{cond,fluid}}} = -\frac{(k_{\text{eff}})_{\text{stagnant}}}{k_{\text{f}}}\frac{\partial T}{\partial X} \tag{15}$$

where

$$Q = -(k_{\text{eff}})_{\text{stagnant}} A \frac{\partial T^*}{\partial x^*}\Big|_{x^*=0} \tag{16}$$

The average Nusselt number along the left wall is calculated by integrating the local Nusselt number over the left wall

$$\overline{Nu} = \int_0^1 Nu\, \mathrm{d}y \tag{17}$$

3. Numerical procedure

The governing equations are discretized with a collocated grid arrangement of the variables following the Rhie

and Chow scheme [18]. The governing equations are solved numerically by finite volume method. The semi-implicit method for pressure linked equation (SIMPLE) [19] is used to couple momentum and continuity equations. The third order accurate deferred QUICK scheme of Hayase et al. [20] is employed to minimize the numerical diffusion for the convective terms for both the momentum equations and the energy equation. The solution of the discretized momentum and pressure correction equation is obtained by TDMA line-by-line method [19]. The iterative procedure is initiated by the solution of energy equation followed by momentum equations and is continued until convergence is achieved. Euclidean norm of the residual is taken as convergence criteria for each dependent variable in the entire flow field [21]. The mass balance for convergence was taken as 10^{-4}. At each time step, the solution is converged and is used in the next time step as initial conditions. Unconditionally stable fully implicit scheme is used to move from nth time step to $(n+1)$th time step. The global convergence criteria is taken as 10^{-4}.

Different values of under relaxation for pressure correction equation and dt are used so that a logical and converged solution can be achieved. At steady state, the error reaches the asymptotic behaviour. Here it is set as sum of temperature error reduced to the steady-state criteria ε

$$\sum_{i,j=1}^{i_{\max},j_{\max}} (T_{i,j}^{n+1} - T_{i,j}^{n}) < \varepsilon \tag{18}$$

4. Validation of the code

To validate the developed code, a two-dimensional lid-driven square-cavity flow problem [22] has been solved and compared. Then the present code is validated for natural convection heat transfer by comparing the results of a buoyancy driven laminar heat transfer in a square cavity with differentially heated side walls. The left wall was kept hot while the right wall was cooled. The top and bottom walls are insulated. In the present work numerical predictions, using the developed algorithm, have been obtained for Rayleigh numbers between 10^3 and 10^6. Table 1 compares the results with those by de Vahl Davis [23], Markatos and Perikleous [24], and Hadjisophocleous et al. [25], Fusegi et al. [26] and Ha and Jung [27]. The computed results are in very good agreement with the benchmark solution.

Iwatsu et al. [10] have solved a mixed convection problem in a square cavity. The top wall is moving with a velocity and maintained at hot condition. The bottom wall is cooled whereas the two vertical walls are under adiabatic condition. The comparison of the results obtained from the present code with those of Iwatsu et al. [10] is shown in Table 2.

There is not much numerical data available in the literature for heat transfer within square cavities using nanofluids. The natural convection problem in a differentially heated square enclosure using nanofluids has been solved and compared the results with those of Santra and Sen [28] (Fig. 2). A very good agreement has been obtained. Khanafer et al. [2] have also solved the same problem with dispersion model. However, the value of constant "C" is not given. So the dispersion model has not been used in the present case though the results have shown almost same pattern (not shown here).

5. Grid independence study

The grid independence test is performed using successively sized grids, 21×21, 41×41, 61×61 and 81×81 for Case I, $Ri = 0.1$ and $\chi = 20\%$. Uniform grid has been used for all the computations. The distribution of the u-velocity in the vertical mid-plane and temperature in the horizontal mid-plane are shown in Fig. 3. It is observed that the curves overlap with each other for 61×61 and 81×81. So a grid number of 61×61 is chosen for further computation. Similar type of grid independence study has been carried out for other cases and not reported here.

6. Results and discussion

Mixed convection flow and temperature fields in a two-sided lid-driven square cavity filled with nanofluid are examined. The numerical code developed in the present investigation is used to carry out a number of simulations for a wide range of the controlling parameters of Ri and χ. The range of Ri for this investigation is varied between $0.1 < Ri < 10$. To vary Ri, Grashof number is fixed at $Gr = 10^4$ while changing Reynolds number through the plate velocity V_p. The calculations are done with Reynolds number identical at both sides of the cavity. The range of χ used in this study is varied between $0 < \chi < 20\%$. The thermophysical properties of fluid and the solid phases are shown in Table 3. Two-sided lid-driven cavity is analyzed according to the direction of moving plate in three cases as shown in Fig. 1. The results for each will be presented next.

Case I: The left wall is moving lid is moving upwards while the right wall moves downwards. It is noted that forces due to the moving lids and the buoyancy act in the opposite directions. The streamlines (on the left) and the isotherms (on the right) for $Ri = 0.1$, 1 and 10 are shown in Figs. 4–6 respectively. For $Ri = 0.1$, Fig. 4 shows that the forced convection plays a dominant role and the recirculation flow is mostly generated only by the moving lids. As can be seen from Fig. 4(a), (c), (e), and (g), the recirculation is clockwise and some perturbations are seen in streamlines in the upper right and lower left corners which is a characteristics of a lid-driven cavity flow problem. It is observed that a strong convection exists in all the cases (Fig. 4(b), (d), (f), and (h)). The strength of the convection increases with χ leading to the thinning of the boundary layers on the vertical walls.

Table 1
Comparison of solutions for natural convection in an enclosed cavity

	a[a]	b[b]	c[c]	d[d]	e[e]	f[f]	$\frac{a-d}{a}*100$
(a) Ra = 10^3							
u_{max}	3.649	3.544	3.544	3.642			0.1918
y	0.813	0.832	0.814	0.804			
v_{max}	3.697	3.593	3.586	3.7026			−0.1514
x	0.718	0.168	0.186	0.1780			
$\overline{Nu}$	1.118	1.108	1.141	1.0871	1.085	1.072	2.76
Nu_{max}	1.505	1.496	1.540	1.508681			0.2750
y	0.092	0.0825	0.142	0.09322			
Nu_{min}	0.692	0.720	0.727	0.6901			0.2745
y	1.0	0.9925	0.991	1.0			
(b) Ra = 10^4							
u_{max}	16.178	16.18	15.995	16.1439			0.2107
y	0.823	0.832	0.814	0.822			
v_{max}	19.617	19.44	18.894	19.6650			−0.244
x	0.119	0.113	0.103	0.110			
$\overline{Nu}$	2.243	2.201	2.29	2.195	2.100	2.070	2.13
Nu_{max}	3.528	3.482	3.84	3.5585			−0.8645
y	0.143	0.1425	0.141	0.1440			
Nu_{min}	0.586	0.643	0.670	0.5809			0.8703
y	1.0	0.9925	0.991	1.0			
(c) Ra = 10^5							
u_{max}	34.73	35.73	37.144	34.30019			1.237
y	0.855	0.857	0.855	0.856			
v_{max}	68.59	169.08	68.91	68.7646			−0.254
x	0.066	0.067	0.061	0.05935			
$\overline{Nu}$	4.519	4.430	4.964	4.450	4.361	4.464	1.52
Nu_{max}	7.117	7.626	8.93	7.9371			−11.523
y	0.081	0.0825	0.080	0.0762			
Nu_{min}	0.729	0.824	1.01	0.71730			1.6049
y	1.0	0.9925	1.0	1.0			
(d) Ra = 10^6							
u_{max}	64.63	68.81	66.42	65.5866			−1.9124
y	0.850	0.872	0.897	0.839			
v_{max}	217.36	221.8	226.4	219.7361			−1.0931
x	0.0379	0.0375	0.0206	0.04237			
$\overline{Nu}$	8.799	8.754	10.39	8.803			−0.00045
Nu_{max}	17.925	17.872	21.41	19.2675			−7.4755
y	0.0378	0.0375	0.030	0.02542			
Nu_{min}	0.989	1.232	1.58	0.9420			4.7522
y	1.0	0.9925	1.0	1.0			

[a] de Vahl Davis [23].
[b] Markatos and Perikleous [24].
[c] Hadjisophocleous et al. [25].
[d] Present solution.
[e] Fusegi et al. [26].
[f] Ha and Jung [27].

Table 2
Comparison of the present data with those of Iwatsu et al. (in bracket) [10]

Re	$Gr = 10^2$	$Gr = 10^4$	$Gr = 10^6$
100	2.10 (1.94)	1.47 (1.34)	1.04 (1.02)
400	3.85 (3.84)	3.61 (3.62)	1.23 (1.22)
1000	6.33 (6.33)	6.28 (6.29)	1.77 (1.77)

For $Ri = 1$ (Fig. 5), the natural convection effect is comparable with the forced convection effect. As a result, two weaker cells are formed at the sides in addition to the main cell (moving at anticlockwise direction). Here the important phenomenon happening is that with the increased concentration inside the fluid, nanofluid helps in minimizing the natural convection effect and precipitate in merging all cells into one for $\chi > 0.08$ (Fig. 5(e)). There is a remarkable chenage in the isotherm pattern from $\chi = 0$ and 0.08 (Fig. 5(b) and (d)) to $\chi = 0.16$ (Fig. 5(f)) and $\chi = 0.20$ (Fig. 5(h)) with the formation of a boundary layer on the vertical walls with accompanying increase in heat transfer. When $Ri = 10$, the effect of natural convection is far more compared to the forced convection effect (Fig. 6). For this

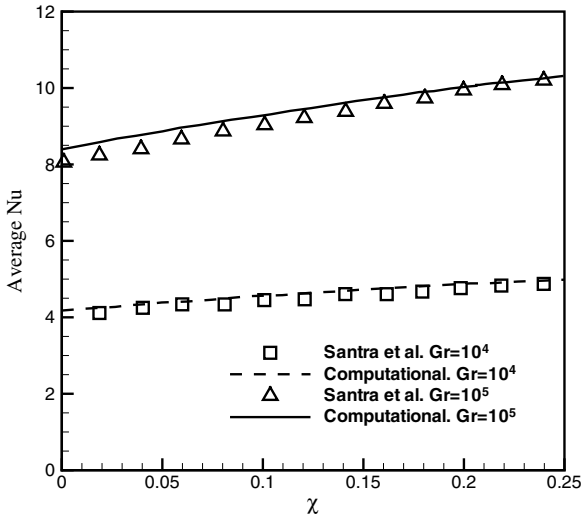

Fig. 2. Validation of the present code with the results of Santra and Sen [28].

case, conditions are strongly favouring the phenomena of natural convection and the effect of nanoparticles is not that much. Thus the streamlines (Fig. 6(a), (c), (e), and (g)) and the isotherms (Fig. 6(b), (d), (f), and (h)) show a similar trend for the range of $\chi = 0$–0.20.

From the mid-plane velocity curves Fig. 13(a) and (c), it can be seen that the solid volume fraction does not have much effect except at $Ri = 1$. This case (Fig. 13(b)) is considerably dependent on the amount of nanoparticles as $\chi > 0.08$, the flow pattern switches from natural convection domination to forced convection domination.

The local Nusselt number (Nu) profile at the left wall has been plotted in Fig. 16. For $Ri = 0.1$, the pattern is similar for all the values of χ. It increases with the increase of χ. For $Ri = 1$, Fig. 16(c) shows that Nu has a sudden increase

Table 3
Thermophysical properties of different phases

Property	Fluid phase (water)	Solid phase (copper)
c_p (J/kg K)	4179	383
ρ (kg/m^3)	997.1	8954
k (W/m K)	0.6	400
β (K^{-1})	2.1×10^{-4}	1.67×10^{-5}

for higher values of χ due to the switching of the flow pattern. For $Ri = 10$, Fig. 16(c) shows a pattern similar to $Ri = 0.1$.

Case II: In this case, the left wall is moving downwards while the right wall is moving upwards, which represents the case of aiding shear and buoyancy forces. Figs. 7–9 show the streamlines (on the left) and isotherms (on the right) for $Ri = 0.1$, 1.0 and 10. As can be seen in Fig. 7, the central vortex is moving anticlockwise direction. The case of $Ri = 0.1$ is of forced convection with smaller buoyancy force where the fluid motion is mainly dictated by the moving boundaries. The formation of the thermal boundary layer on the two vertical walls can be noticed. For $Ri = 1$ (Fig. 8), the central core consists of two small vortices when $\chi = 0$, i.e., for base fluid (Fig. 8(a)). However, as χ increases, the heat transfer increases as the thermal boundary layers are getting thinner. These vortices coalesce into one single core at the center (Fig. 8(c), (e), and (g)). The formation of the thermal boundary layers for all the χ's is to be noticed here. At $Ri = 10$ (Fig. 9(a), (c), (e), and (g)), the flow is characterized by the large central main eddy breaking into two small eddies at the core. Unlike for $Ri = 1.0$, they cannot coalesce into one even with increased χ because of the increased natural convection strength. The thermal boundary layer spreads out more in the flow direction (Fig. 9(b), (d), (f), (h)). For $Ri = 0.1$ and 10, velocity at mid plane is decreasing with increasing solid volume

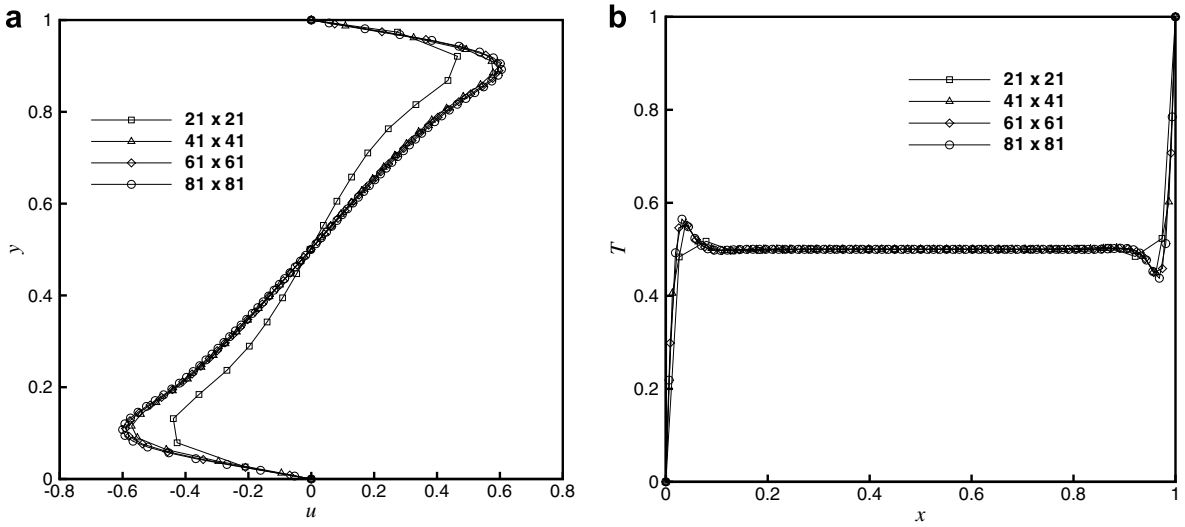

Fig. 3. Grid independence test for case I, $Ri = 0.1$ and $\chi = 20\%$: (a) u-velocity distribution in the vertical mid-plane and (b) temperature distribution in the horizontal mid-plane.

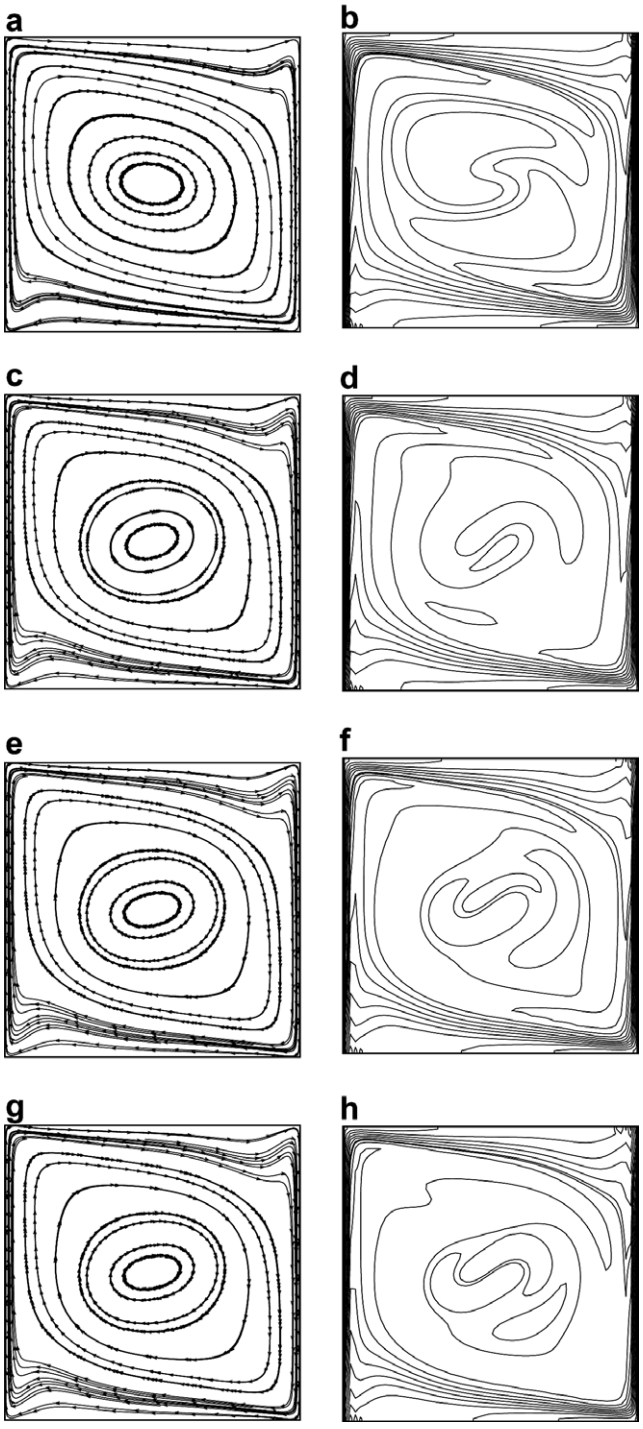

Fig. 4. Streamlines (a, c, e, g) and isotherms (b, d, f, h) for Case I and $Ri = 0.1$: (a) $\chi = 0\%$; (b) $\chi = 0\%$; (c) $\chi = 8\%$; (d) $\chi = 8\%$; (e) $\chi = 16\%$; (f) $\chi = 16\%$; (g) $\chi = 20\%$; (h) $\chi = 20\%$.

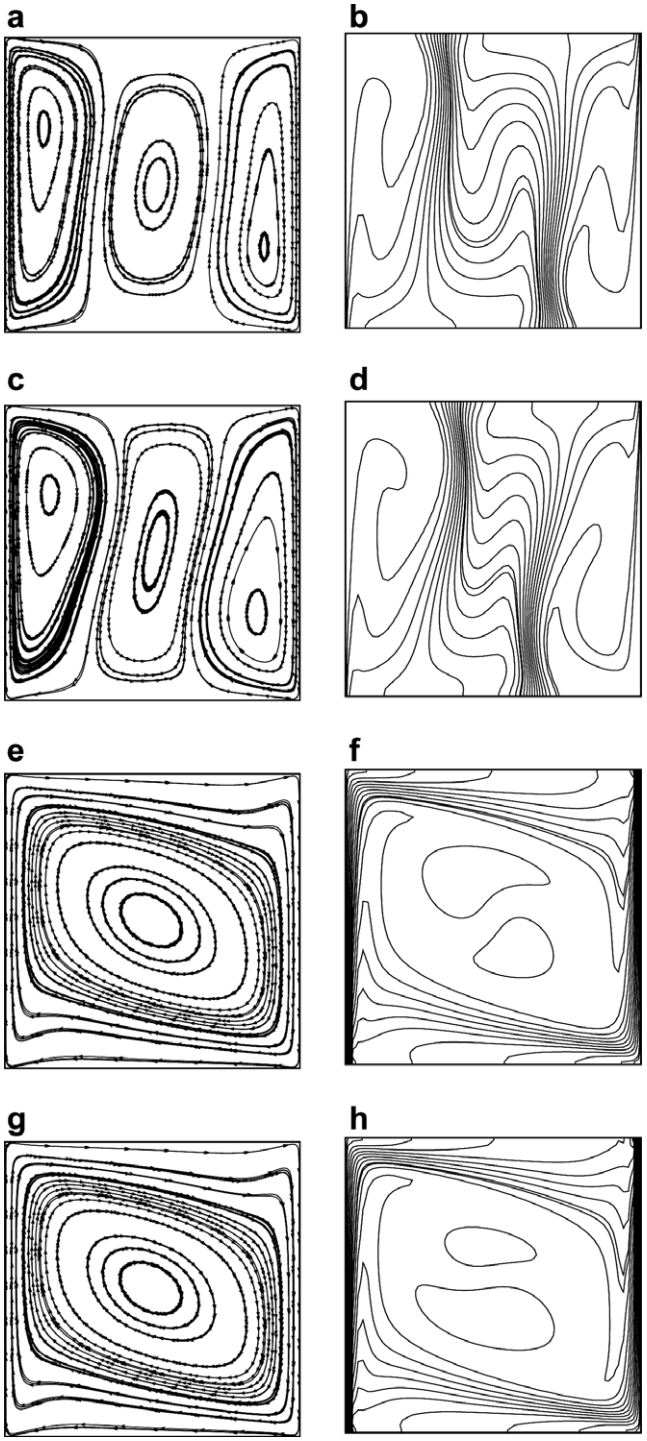

Fig. 5. Streamlines and isotherms for Case I and $Ri = 1$: (a) $\chi = 0\%$; (b) $\chi = 0\%$; (c) $\chi = 8\%$; (d) $\chi = 8\%$; (e) $\chi = 16\%$; (f) $\chi = 16\%$; (g) $\chi = 20\%$; (h) $\chi = 20\%$.

fraction while opposite happens for $Ri = 1$ (Fig. 14). In Fig. 17, the Nusselt number profile at the left wall is plotted. For all the values of Ri, the pattern is almost similar. With increasing χ, the Nusselt number is increasing.

Case III: This is the case where both the vertical walls move upward in which the buoyancy and shear forces are aiding each other on the right wall and opposite situation happens on the left wall. Therefore it is expected that the main circulation will be on the right side of the cavity. Streamlines and isotherms for $Ri = 0.1$, 1.0 and 10 are presented in Figs. 10–12 respectively. For $Ri = 0.1$, it is seen that there is a large counter-clockwise circulating eddy at the right hand side and a small clockwise circulating eddy at the left side (Fig. 10(a), (c), (e), (g)). This behaviour is

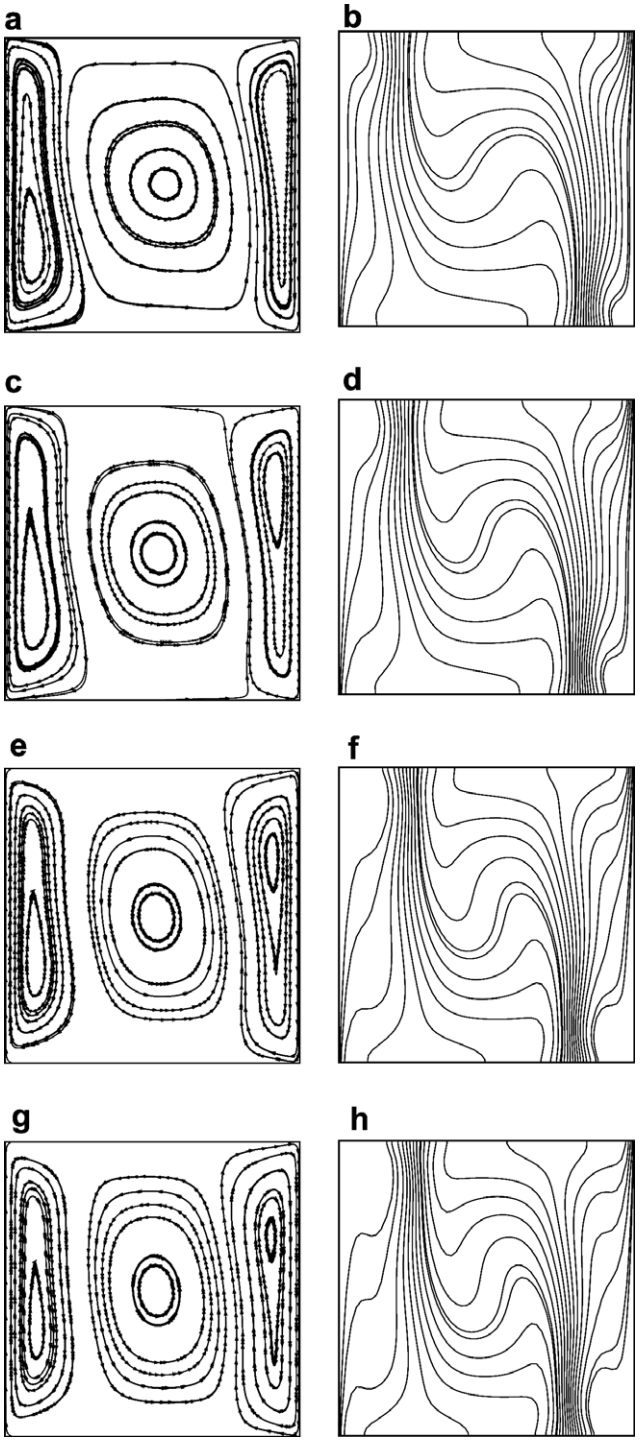

Fig. 6. Streamlines and isotherms for Case I and $Ri = 10$: (a) $\chi = 0\%$; (b) $\chi = 0\%$; (c) $\chi = 8\%$; (d) $\chi = 8\%$; (e) $\chi = 16\%$; (f) $\chi = 16\%$; (g) $\chi = 20\%$; (h) $\chi = 20\%$.

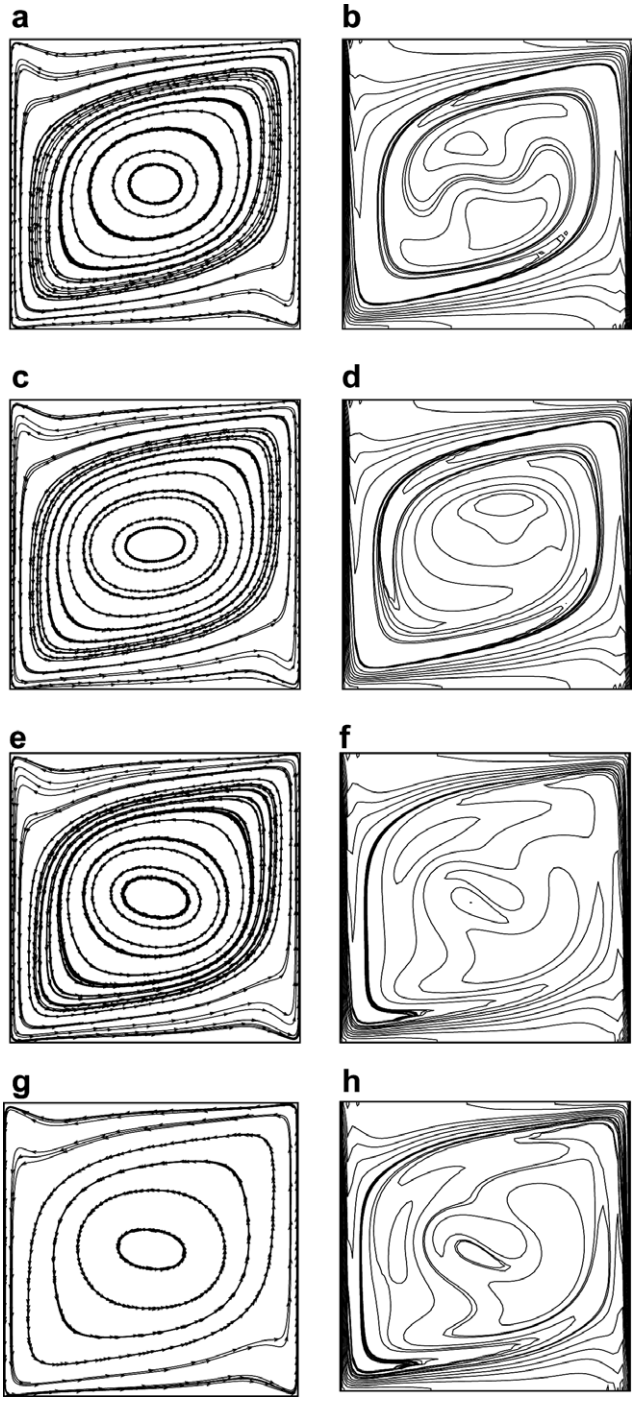

Fig. 7. Streamlines and isotherms for Case II and $Ri = 0.1$: (a) $\chi = 0\%$; (b) $\chi = 0\%$; (c) $v = 8\%$; (d) $\chi = 8\%$; (e) $\chi = 16\%$; (f) $\chi = 16\%$; (g) $\chi = 20\%$; (h) $\chi = 20\%$.

very logical because the forced convection is dominant and the buoyancy force is negligible. The eddy on the right side is dominant because of the aiding buoyancy and shear forces. Isotherms for this case (Fig. 10(b), (d), (f), (h)) form a steeper thermal gradients between the two counter-circulating eddies and no temperature gradient penetration is discernable around them. For $Ri = 1$ (Fig. 11), the aiding buoyancy driven force on the right wall affects the flow and temperature fields while that on the left is almost nullified by the opposing shear forces. As a result, the cell on the right fills the cavity more than the one on the left. For $Ri = 10$ (Fig. 12), which is a buoyancy dominated regime, the counter clockwise circulating cell on the right grows further due to the aiding forces on the hot wall while the one on the left becomes weaker and smaller, i.e., the left cell

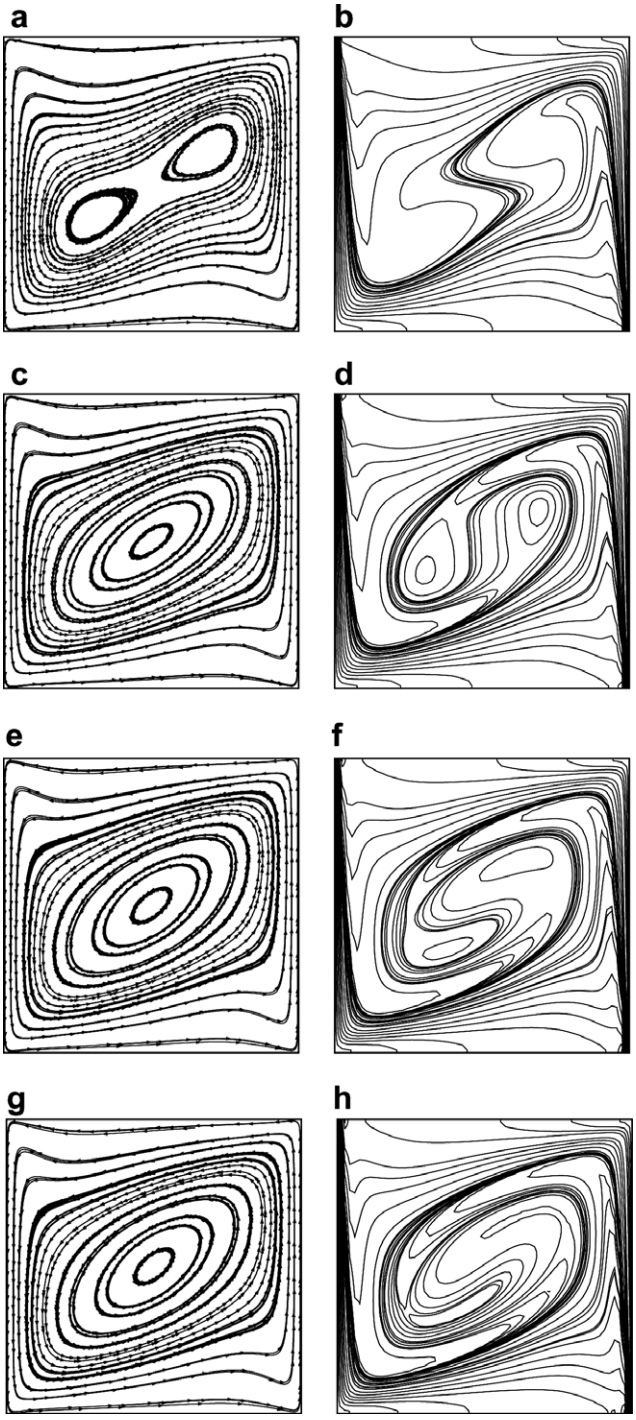

Fig. 8. Streamlines and isotherms for Case II and $Ri = 1$: (a) $\chi = 0\%$; (b) $\chi = 0\%$; (c) $\chi = 8\%$; (d) $\chi = 8\%$; (e) $\chi = 16\%$; (f) $\chi = 16\%$; (g) $\chi = 20\%$; (h) $\chi = 20\%$.

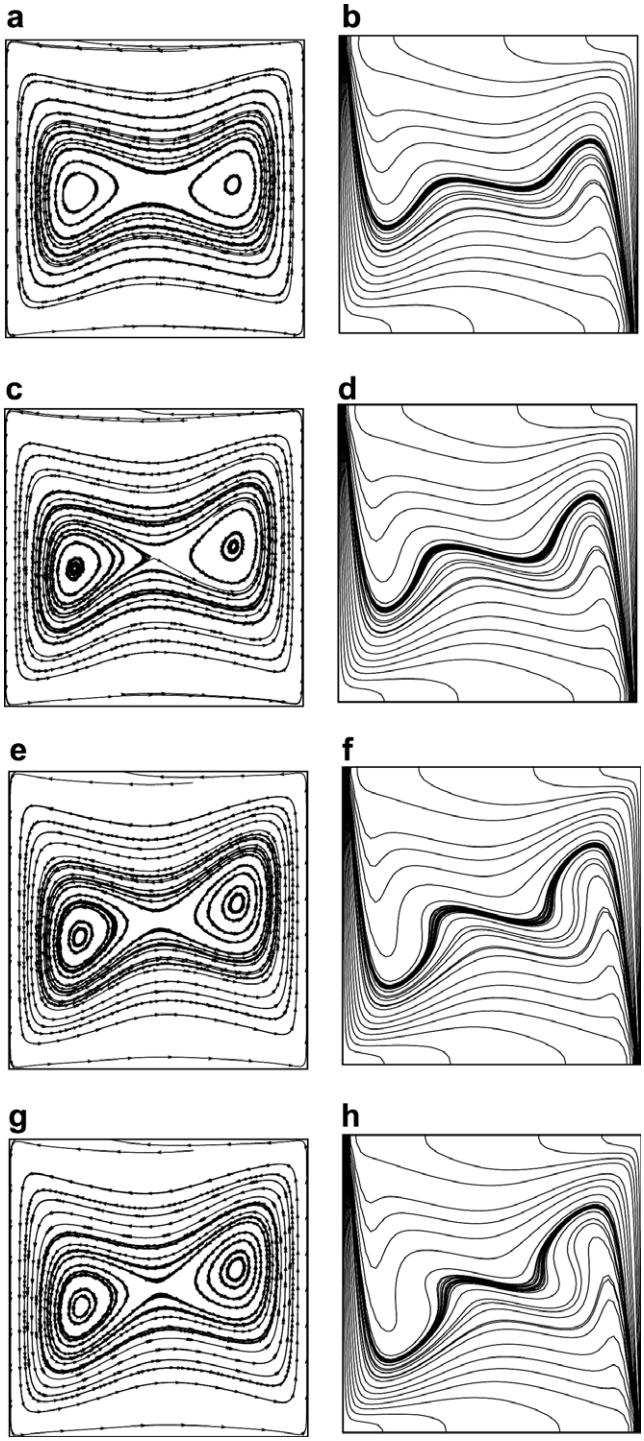

Fig. 9. Streamlines and isotherms for Case II and $Ri = 10$: (a) $\chi = 0\%$; (b) $\chi = 0\%$; (c) $\chi = 8\%$; (d) $\chi = 8\%$; (e) $\chi = 16\%$; (f) $\chi = 16\%$; (g) $\chi = 20\%$; (h) $\chi = 20\%$.

nearly vanishes for the natural convection becomes more dominant there. The effect of the right wall (moving upward) in this case becomes negligibly small as if it were not moving. The isotherms (Fig. 12(b), (d), (f), and (h)) are like those observed in natural convection in differentially heated cavities and show steeper horizontal temperature gradients at the lower part of the right moving wall. Due to the presence of the left cell, the temperature gradient is weakened at the center of the cavity and a stratification is observed. From Fig. 15, it can be seen that with increasing χ, the mid plane velocity decreases.

The Nusselt number profile at the left wall is plotted in Fig. 18. For $Ri = 0.1$ and 1 the pattern is similar, Nusselt

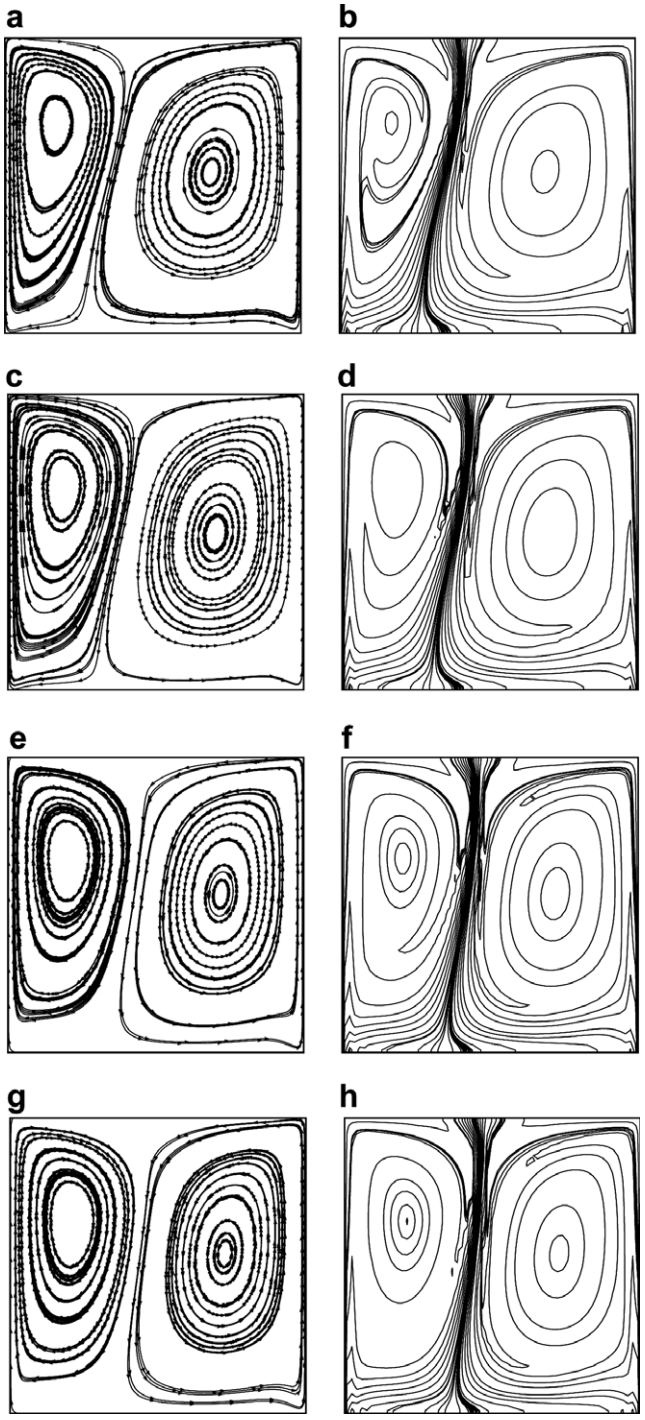

Fig. 10. Streamlines and isotherms for Case III and $Ri = 0.1$: (a) $\chi = 0\%$; (b) $\chi = 0\%$; (c) $\chi = 8\%$; (d) $\chi = 8\%$; (e) $\chi = 16\%$; (f) $\chi = 16\%$; (g) $\chi = 20\%$; (h) $\chi = 20\%$.

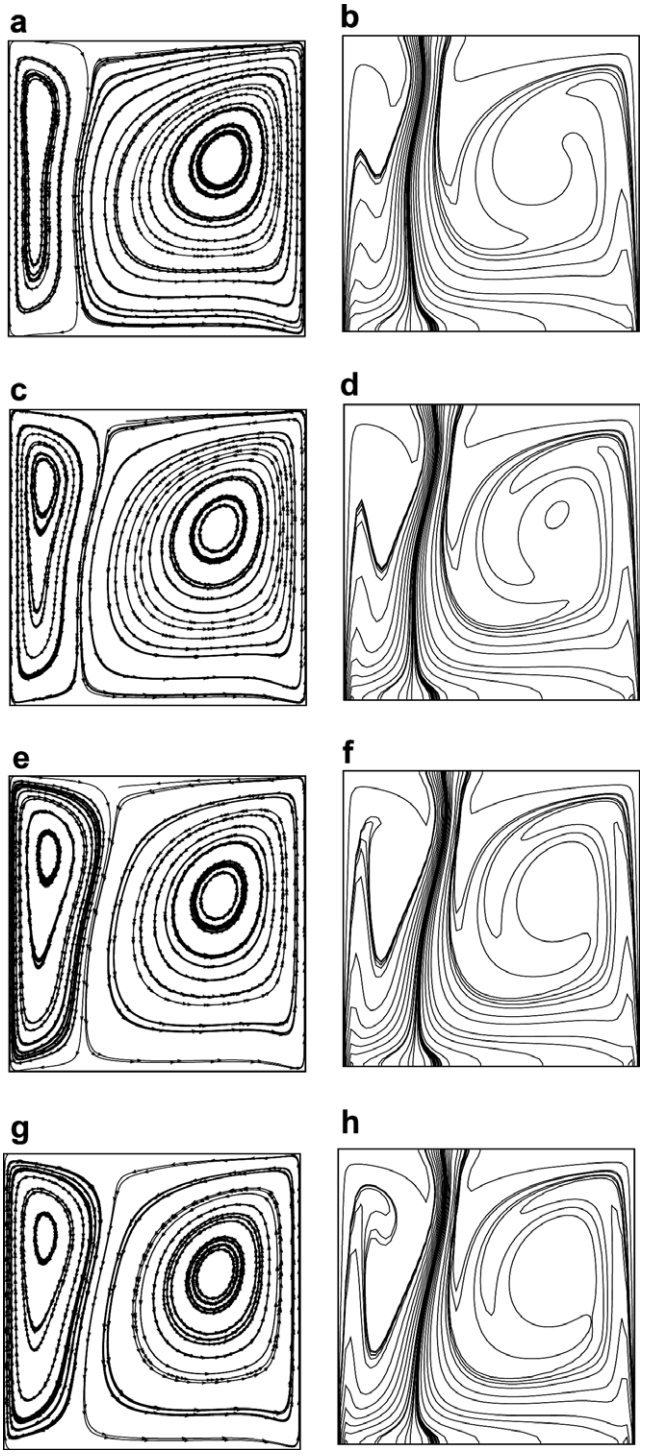

Fig. 11. Streamlines and isotherms for Case III and $Ri = 1$: (a) $\chi = 0\%$; (b) $\chi = 0\%$; (c) $\chi = 8\%$; (d) $\chi = 8\%$; (e) $\chi = 16\%$; (f) $\chi = 16\%$; (g) $\chi = 20\%$; (h) $\chi = 20\%$.

number increases with χ. For $Ri = 10$ (Fig. 11(c)), at the top portion of wall, the Nusselt number is not varying that much but at the lower portion it changes very fast. This is well expected as can be seen in the respective isotherm plots that at lower part of the wall the temperature gradient is sharp.

Overall heat transfer: The average Nusselt number ($\overline{Nu}$) for three cases and different Richardson number are calculated using Eq. (17) and presented in Fig. 19. Fig. 19(a) shows that with increasing χ, the heat transfer capacity of media also increases but for $Ri = 1$, $\overline{Nu}$ dramatically changes when χ is increased from 0.08 to 0.16. This is because here nanoparticles are capable of changing the flow feature.

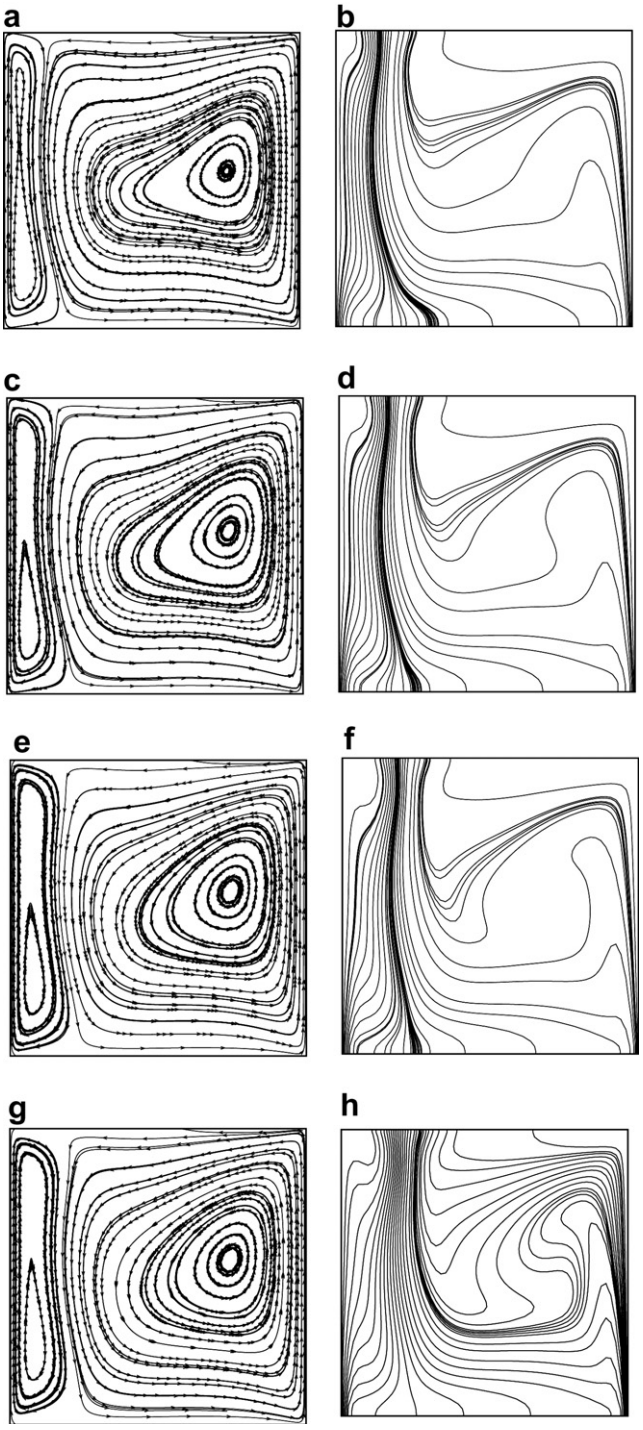

Fig. 12. Streamlines and isotherms for Case III and $Ri = 10$: (a) $\chi = 0\%$; (b) $\chi = 0\%$; (c) $\chi = 8\%$; (d) $\chi = 8\%$; (e) $\chi = 16\%$; (f) $\chi = 16\%$; (g) $\chi = 20\%$; (h) $\chi = 20\%$.

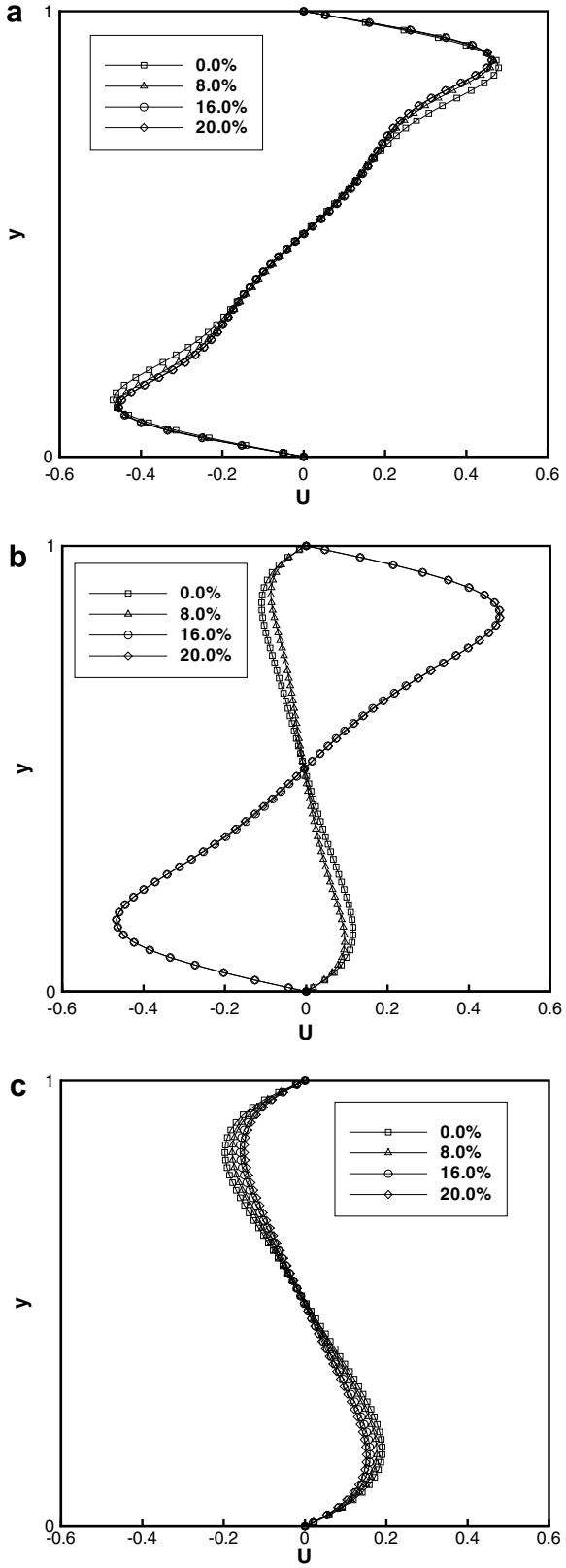

Fig. 13. Case I: mid-plane u-velocity: (a) $Ri = 0.1$; (b) $Ri = 1$; (c) $Ri = 10$.

For case II, from Fig. 19(b) the Nusselt number is clearly increasing with solid volume fraction for all the values of Richardson number. For $Ri = 0.1$ it is changing from 30 to 70 which clearly demonstrates their superior capability as heat transfer media. For case III, Fig. 19(b) shows that increase in χ increases the average Nusselt number. It should be noted that the trend in Fig. 19 for the average Nusselt number versus the volume fraction would be downward if the Nusselt number is based on the effective

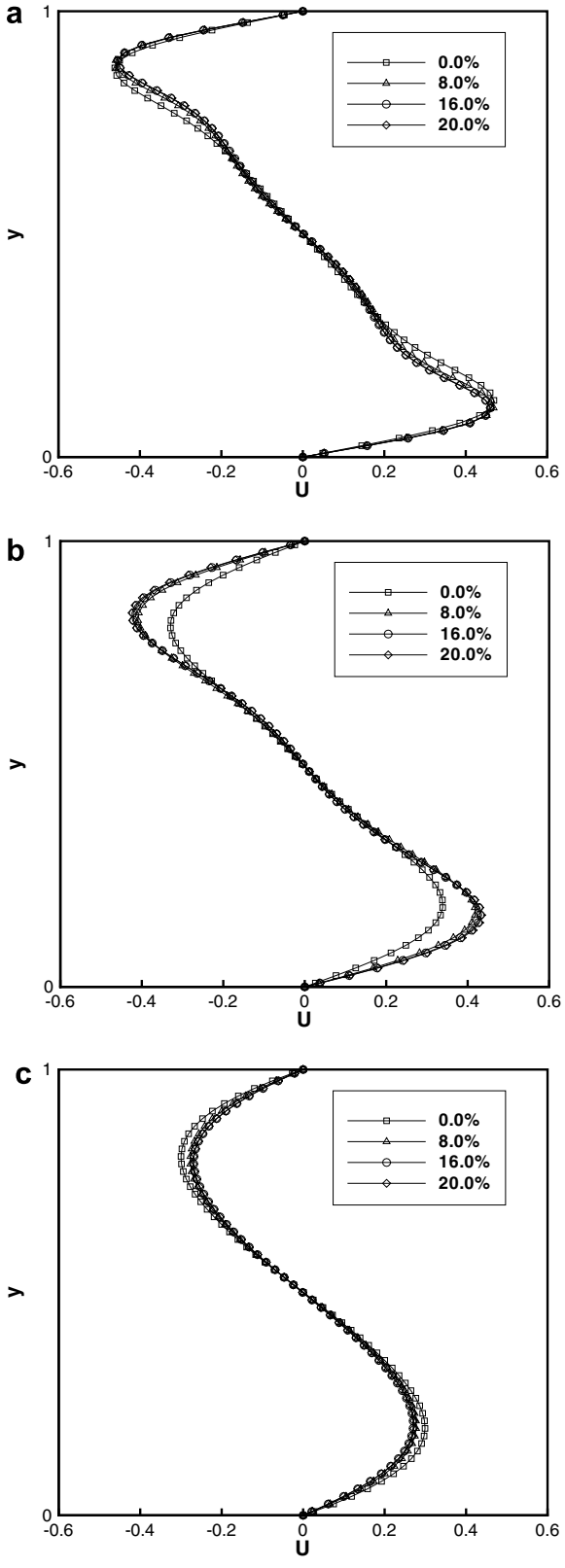

Fig. 14. Case II: mid-plane u-velocity: (a) $Ri = 0.1$; (b) $Ri = 1$; (c) $Ri = 10$.

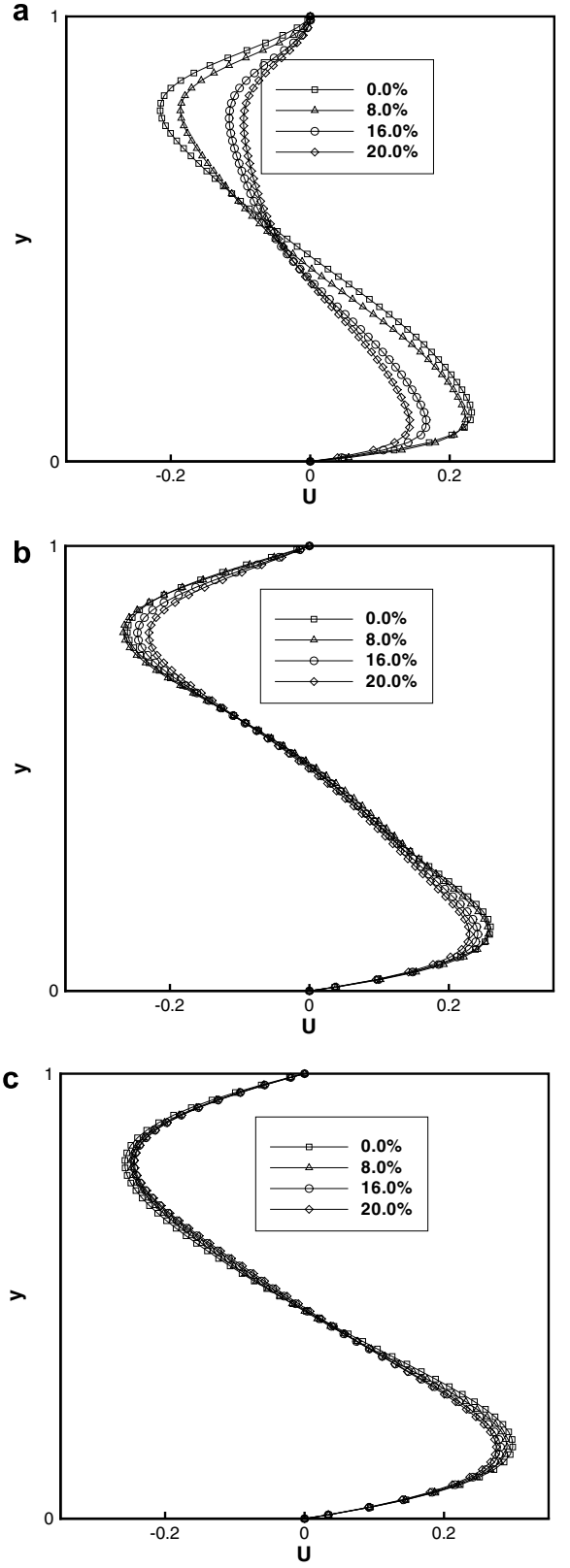

Fig. 15. Case III: mid-plane u-velocity: (a) $Ri = 0.1$; (b) $Ri = 1$; (c) $Ri = 10$.

thermal conductivity, k_{eff}, instead of the fluid thermal conductivity, k_{f}.

The variations of average Nusselt number ($\overline{Nu}$) with Ri and χ for the three cases are shown in Table 4. For Case I (Table 4(a)), $Ri = 1$, there is a substantial increase in $\overline{Nu}$ as χ is increased above 8%. In general, Nu increases with χ. When χ is 8%, the increase is approximately 30%. When

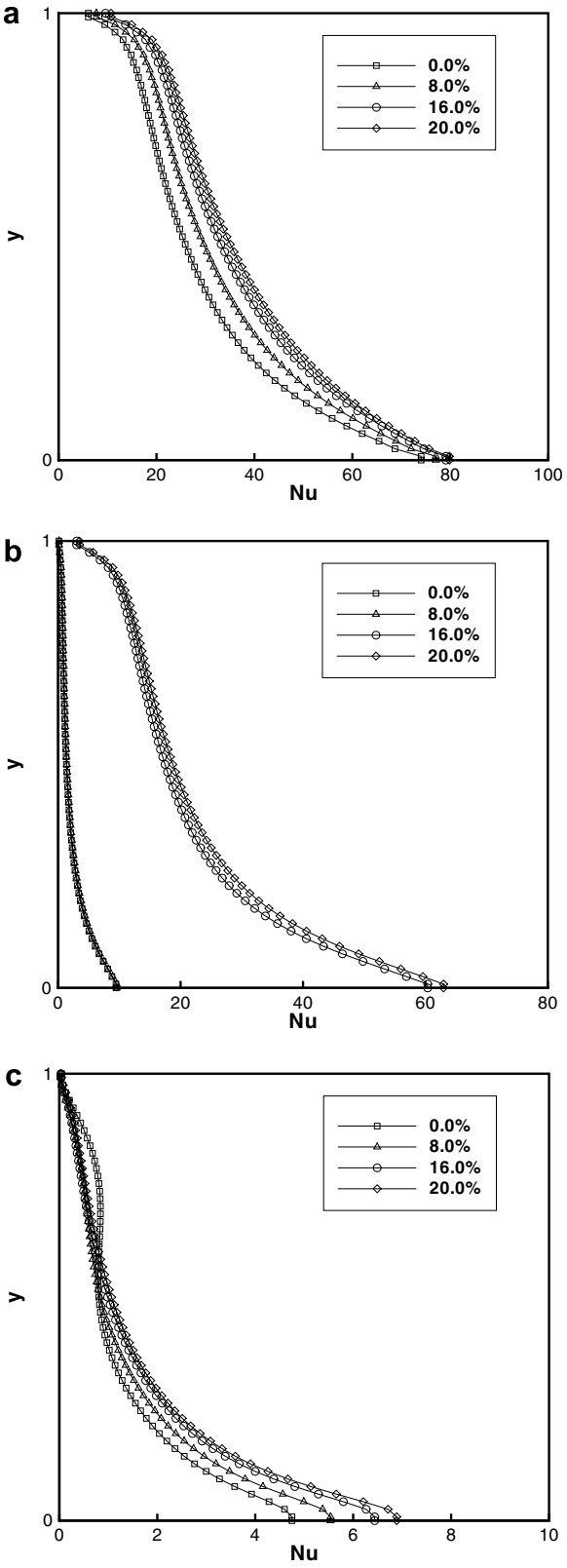

Fig. 16. Case I: local Nusselt number at wall: (a) $Ri = 0.1$; (b) $Ri = 1$; (c) $Ri = 10$.

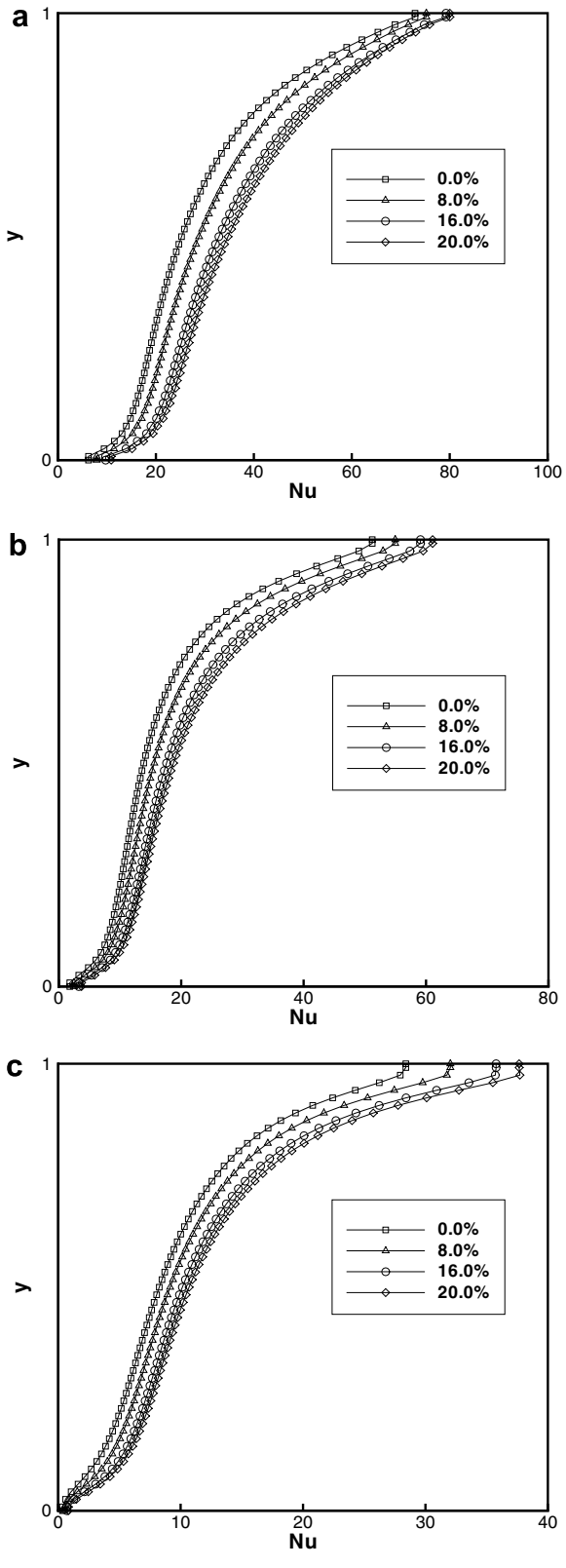

Fig. 17. Case II: local Nusselt number at wall: (a) $Ri = 0.1$; (b) $Ri = 1$; (c) $Ri = 10$.

χ is 16%, the increase is approximately 90%. When χ is 20%, the increase is above 100%. For case II (Table 4(b)), as χ is increased to 8%, an increase of 40% is observed. A heat transfer augmentation of above 90% is obtained for $\chi = 0.16$ compared to $\chi = 0.0$. This value becomes more than 125% as χ becomes 20%. For case III

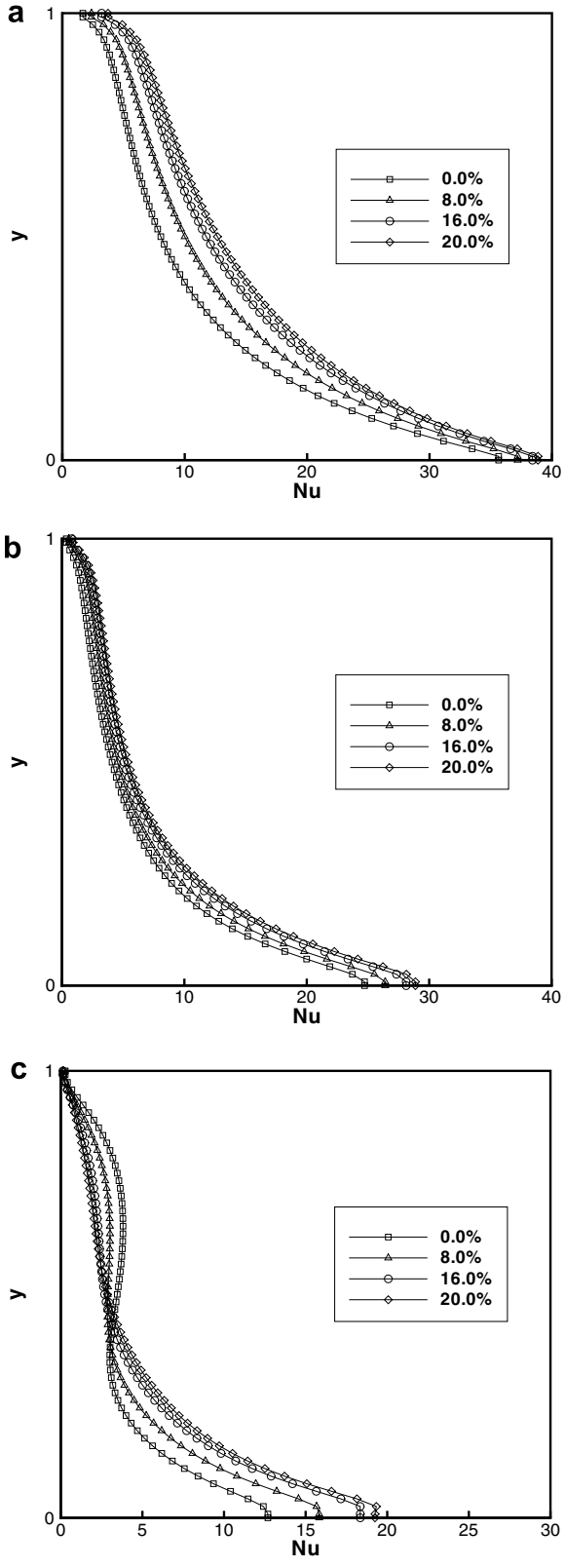

Fig. 18. Case III: local Nusselt number at wall: (a) $Ri = 0.1$; (b) $Ri = 1$; (c) $Ri = 10$.

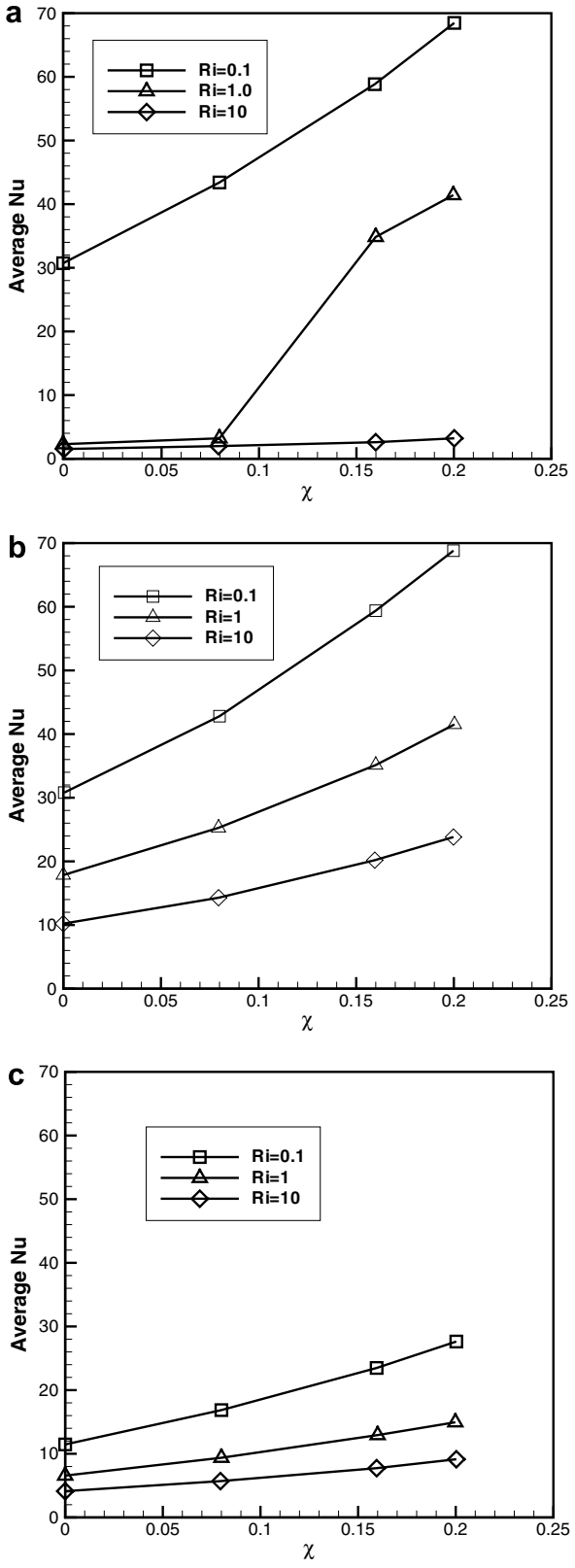

Fig. 19. Nusselt Number comparisons for the three cases: (a) Case I; (b) Case II; (c) Case III.

(Table 4(c)), $\overline{Nu}$ is more for $Ri = 0.1$ compared to $Ri = 10.0$. As χ is increased to 0.08, the increase is little above 30%. An increment of 80% or more is observed when χ is increased to 0.16. For $\chi = 0.2$, an increase of 110% or more is observed for the three Ri.

Table 4
Comparison of average Nusselt number ($\overline{Nu}$) for three cases and various solid volume fractions

	A ($\chi = 0\%$)	B ($\chi = 8\%$)	% Increase[a]	D ($\chi = 16\%$)	% Increase[b]	F ($\chi = 20\%$)	% Increase[c]
(a) Case I							
$Ri = 0.1$	30.68	43.16	40.70	58.86	91.88	68.43	123.06
$Ri = 1$	2.36	3.08	30.60	34.74	1373.16	41.31	1651.38
$Ri = 10$	1.38	1.85	33.55	2.63	89.81	3.14	126.5
(b) Case II							
$Ri = 0.1$	30.67	42.78	39.50	59.40	93.69	69.03	125.09
$Ri = 1$	17.96	25.22	40.44	35.22	96.10	41.51	131.10
$Ri = 10$	10.19	14.45	41.80	20.19	98.10	23.79	133.35
(c) Case III							
$Ri = 0.1$	11.54	16.81	45.65	23.44	103.15	27.50	138.30
$Ri = 1$	6.65	9.28	39.53	12.76	91.92	14.92	124.38
$Ri = 10$	4.25	5.70	33.93	7.62	79.16	9.03	112.29

[a] $\frac{B-A}{A} \times 100$.
[b] $\frac{D-A}{A} \times 100$.
[c] $\frac{F-A}{A} \times 100$.

7. Conclusions

This study has been concerned with the numerical modeling of mixed convection in two-sided lid-driven differentially heated square cavity filled with nanofluid. It has been performed for three different cases characterized by the direction of movement of the vertical walls. The governing parameters are Ri and χ.

In view of the results, following findings may be summarized.

1. The nanoparticles when immersed in a fluid are capable of increasing the heat transfer capacity of base fluid. As solid volume fraction increases, the effect is more pronounced. The variation of average Nusselt number is nonlinear with solid volume fraction.
2. Nanoparticles are able to change the flow pattern of a fluid from natural convection to forced convection regime. For Case I, it is found that nanoparticles after a certain limit can increase the Nusselt number drastically for $Ri = 1.0$.
3. When both the vertical walls move upwards in the same direction (i.e. Case III), the heat transfer is reduced compared to the other two cases (Cases I and II). This is observed for $Ri = 0.1$, 1 and 10.0.
4. In the case of $Ri < 1$, which is the forced convection dominated regime, when the vertical walls move in opposite direction, cases I and II, the heat transfer is considerably enhanced regardless of which side moves upwards. For $Ri = 1.0$, $\overline{Nu}$ is high for Case II compared to Cases I and III. For $\chi = 0.16$ and 0.20, $\overline{Nu}$ is smaller for Cases I and II.
5. For Case I, $Ri = 1$, there is a substantial increase in $\overline{Nu}$ as χ is increased above 8%. In general, $\overline{Nu}$ increases with χ. When χ is 0.08, the increase is approximately 30%. When χ is 0.16, the increase is approximately 90%. When χ is 0.2, the increase is above 100%.

References

[1] J.A. Eastman, S.U.S. Choi, S. Li, W. Yu, L.J. Thompson, Anamolously increased effective thermal conductivities of ethylene glycol-based nanofluids containing copper nanoparticles, Phys. Lett. Appl. 78 (6) (2001) 718–720.
[2] K. Khanafer, K. Vafai, M. Lightstone, Buoyancy driven heat transfer enhancement in a two-dimensional enclosure utilizing nanofluids, Int. J. Heat Mass Transfer 46 (2003) 3639–3653.
[3] A. Amiri, K. Vafai, Analysis of dispersion effects and non-thermal equilibrium, non-Darcian, variable porosity incompressible flow through porous media, Int. J. Heat Mass Transfer 37 (1994) 939–954.
[4] A.-R.A. Khaled, K. Vafai, Heat transfer enhancement through control of thermal dispersion effects, Int. J. Heat Mass Transfer 48 (2005) 2172–2185.
[5] R. Chein, G. Huang, Analysis of microchannel heat sink performance using nanofluids, Appl. Thermal Eng. 25 (2005) 3104–3114.
[6] J. Koo, C. Kleinstreuer, Laminar nanofluid flow in microheat-sinks, Int. J. Heat Mass Transfer 48 (2005) 2652–2661.
[7] G. Roy, C.T. Nguyen, P.-R. Lajoie, Numerical investigation of laminar flow and heat transfer in a radial flow cooling system with the use of nanofluids, Superlattices Microstruct. 35 (2004) 497–511.
[8] S.E.B. Maiga, C.T. Nguyen, N. Galanis, G. Roy, Heat transfer behaivours of nanofluids in a uniformly heated tube, Superlattices Microstruct. 35 (2004) 543–557.
[9] S.E.B. Maiga, S.J. Palm, C.T. Nguyen, G. Roy, N. Galanis, Heat transfer enhancement by using nanofluids in forced convection flows, Int. J. Heat Fluid Flow 26 (2005) 530–546.
[10] R. Iwatsu, J.M. Hyun, K. Kuwahara, Mixed convection in a driven cavity with a stable vertical temperature gradient, Int. J. Heat Mass Transfer 36 (1993) 1601–1608.
[11] H.F. Oztop, I. Dagtekin, Mixed convection in two-sided lid-driven differentially heated square cavity, Int. J. Heat Mass Transfer 47 (2004) 1761–1769.
[12] R.-Y. Jou, S.-C. Tzeng, Numerical research on nature convective heat transfer enhancement filled with nanofluids in rectangular enclosures, Int. Commun. Heat Mass Transfer 33 (2006) 727–736.

[13] J.C. Maxwell, A Treatise on Electricity and Magnetism, second ed., Oxford University Press, Cambridge, 1904, pp. 435–441.
[14] R.L. Hamilton, O.K. Crosser, Thermal conductivity of heterogeneous two-component systems, Ind. Eng. Chem.: Fundam. 1 (1962) 182–191.
[15] H.C. Brinkman, The viscosity of concentrated suspensions and solutions, J. Chem. Phys. 20 (1952) 571–581.
[16] Y. Xuan, Q. Li, Report of Nanjing University of Sciences and Technology, 1999 (in Chinese).
[17] Y. Xuan, Q. Li, Investigation on convective heat transfer and flow features of nanofluids, ASME J. Heat Transfer 125 (2003) 151–155.
[18] C.M. Rhie, W.L. Chow, A numerical study of the turbulent flow past an isolated airfoil with trailing edge separation, AIAA J. 21 (1983) 1525–1532.
[19] S.V. Patankar, Numer. Heat Transfer Fluid Flow, Hemisphere Publication Company, NY, 1980, ISBN 0-07-048740-5.
[20] T. Hayase, J.A.C. Humphrey, R. Greif, A consistently formulated QUICK scheme for fast and stable convergence using finite-volume iterative calculation procedures, J. Comput. Phys. 98 (1990) 108–118.
[21] J.P. Van Doormaal, G.D. Raithby, Enhancements of the SIMPLE method for predicting incompressible fluid flows, Numer. Heat Transfer: Part A 7 (1984) 147–163.
[22] U. Ghia, K.N. Ghia, C.T. Shin, High Re solutions for incompressible flow using the Navier–Stokes equations and multigrid method, J. Comput. Phys. 48 (1982) 387–411.
[23] G. de Vahl Davis, Natural convection of air in a square cavity: a benchmark solution, Int. J. Numer. Methods Fluids 3 (1983) 249–264.
[24] N.C. Markatos, K.A. Pericleous, Laminar and turbulent natural convection in an enclosed cavity, Int. J. Heat Mass Transfer 27 (5) (1984) 755–772.
[25] G.V. Hadjisophocleous, A.C.M. Sousa, J.E.S. Venart, Predicting the transient natural convection in enclosures of arbitrary geometry using a nonorthogonal numerical model, Numer. Heat Transfer: Part A 13 (1998) 373–392.
[26] T. Fusegi, K. Kuwahara, B. Farouk, A numerical study of three-dimensional natural convection in a differentially heated cubic enclosure, Int. J. Heat Mass Transfer 34 (6) (1991) 1543–1557.
[27] M.Y. Ha, M.J. Jung, A numerical study of three-dimensional conjugate heat transfer of natural convection and conduction in a differentially heated cubic enclosure with a heat-generating cubic conducting body, Int. J. Heat Mass Transfer 43 (2000) 4229–4248.
[28] A.K. Santra, S. Sen, N. Chakraborty, Analysis of laminar natural convection in a square cavity using nanofluid, in: 31st National Conference on FMFP, Jadavpur University Kolkata, December 2004, pp. 240–248.